



## **Ammonia-methane interaction in jet-stirred and flow reactors: An experimental and kinetic modeling study**

Suphaporn Arunthanayothin, Alessandro Stagni, Yu Song, Olivier Herbinet,  
Tiziano Faravelli, Frederique Battin-Leclerc

### **► To cite this version:**

Suphaporn Arunthanayothin, Alessandro Stagni, Yu Song, Olivier Herbinet, Tiziano Faravelli, et al..  
Ammonia-methane interaction in jet-stirred and flow reactors: An experimental and kinetic modeling study.  
Proceedings of the Combustion Institute, 2021, <10.1016/j.proci.2020.07.061>. <hal-03196454>

**HAL Id: hal-03196454**

**<https://hal.science/hal-03196454v1>**

Submitted on 12 Apr 2021

**HAL** is a multi-disciplinary open access archive for the deposit and dissemination of scientific research documents, whether they are published or not. The documents may come from teaching and research institutions in France or abroad, or from public or private research centers.

L'archive ouverte pluridisciplinaire **HAL**, est destinée au dépôt et à la diffusion de documents scientifiques de niveau recherche, publiés ou non, émanant des établissements d'enseignement et de recherche français ou étrangers, des laboratoires publics ou privés.



HAL Authorization

# Ammonia–methane interaction in jet-stirred and flow reactors: An experimental and kinetic modeling study

Suphaporn Arunthanayothin<sup>a</sup>, Alessandro Stagni<sup>b</sup>, Yu Song<sup>a,c</sup>, Olivier Herbinet<sup>a</sup>,  
Tiziano Faravelli<sup>b</sup>, Frédérique Battin-Leclerc<sup>a</sup>

<sup>a</sup> *Université de Lorraine, CNRS, LRGP, F-54000 Nancy, France*

<sup>b</sup> *CRECK Modeling Lab, Department of Chemistry, Materials and Chemical Engineering “G. Natta”,  
Politecnico di Milano, P.zza Leonardo da Vinci 32, 20133 Milano, Italy*

<sup>c</sup> *Laboratoire PRISME, Université d’Orléans, Polytech Vinci – 45072 Orléans cedex, France*

Published in *Proceedings of the Combustion Institute* 38 (2021) 345-353

## Abstract

The influence of the addition of ammonia on the oxidation of methane was investigated both experimentally and numerically. Experiments were carried out at atmospheric pressure, using a fused silica jet-stirred reactor, and a recrystallized alumina tubular reactor designed on purpose to reach temperatures as high as  $\sim 2000$  K. A temperature range of 600–1200 K was investigated in the jet-stirred reactor at a residence time of 1.5 s, while experiments in the flow reactor were carried out between 1200 and 2000 K, for a fixed residence time of about 25 ms in the reactive zone. A methane/ammonia mixture, diluted in helium, was used in both reactors with equivalence ratios varied between 0.5 and 2 in the first reactor, while stoichiometric conditions were investigated in the second one. The measurements indicate that  $\text{CH}_4$  reactivity was promoted by  $\text{NH}_3$  addition below 1200 K, but not so much influenced above. These results were interpreted and explained using a comprehensive kinetic model, previously validated over a wider range of operating conditions. The mechanism allowed to shed light on the underlying causes of the anticipated methane reactivity at low temperature, and of the major role played by  $\text{NO}_x$  in it. This effect was shown to become less significant at higher temperatures, where the reactivity is mainly governed by H-abstractions on both fuels.

**Keywords:** Ammonia, Jet-stirred reactor, Flow reactor, Oxidation, Detailed kinetic modeling.

## 1. Introduction

Nowadays, a great attention is being paid to the gas-phase oxidation of ammonia, either as pure or mixed with other hydrocarbons. Ammonia is one of the components of biogas, a potentially renewable fuel produced via the anaerobic digestion of organic feedstocks. Biogas is primarily composed of methane and carbon dioxide, with smaller amounts of water, nitrogen, oxygen, ammonia and hydrogen sulfide. Its relative composition varies according to the original source [1,2], which may have an influence on the reactivity and the pollutant formation when biogas is used as a fuel. In addition, ammonia is a potentially carbon-free fuel, which could be used, like hydrogen, as a flexible energy carrier, with applications in several industrial sectors [3]. Therefore, it has the potential to store excess energy, and unlock the vast potential of intermittent renewable energy (e.g. wind, sun [4]). Due to its weak combustion properties, co-firing of ammonia with a combustion enhancer (e.g. hydrogen, methane or coal) is one of the proposed solutions to allow its use in gas turbines, engines or industrial furnaces [3,5,6]. Whatever the application domain, a comprehensive understanding of ammonia combustion characteristics and its mutual interaction with species like methane is essential for designing efficient industrial processes and controlling undesired emissions. Indeed, the presence of nitrogen in the molecule makes ammonia kinetics intrinsically related to the formation of Nitrogen Oxides (NO<sub>x</sub>), either as fuel or intermediate species (e.g. organic fuels containing nitrogen).

The literature is very rich in experimental data for neat methane and neat ammonia [7], but much less is available with regard to the oxidation of ammonia–methane mixtures, in spite of the growing interest. Most of ammonia–methane oxidation studies were performed in premixed flames (e.g., [8,9]) with a focus on the detection of flame intermediates [10–12], or on the measurements of adiabatic burning velocities [13,14]. Previous studies were also carried out in flow reactors [15,16] where the oxidation of NH<sub>3</sub>/CH<sub>4</sub> mixtures in N<sub>2</sub> or CO<sub>2</sub> environments was investigated, at atmospheric pressure and intermediate/high-temperatures with NO, CO and CO<sub>2</sub> quantification. Other studies on the oxidation of methane doped with ammonia using CO<sub>2</sub> as bath gas were performed in flames [8,17–19]. Several detailed kinetic models were proposed to account for the oxidation chemistry of ammonia/methane mixtures, and to investigate the mutual interaction between the two fuels [8,15,20,21].

In order to better understand ammonia–methane interaction in a wider range of operating temperature conditions, we performed experimental campaigns using two different configurations, respectively a Jet-Stirred Reactor (JSR) and a Flow Reactor (FR), such as to cover low-, intermediate- and high-temperature conditions. A detailed analysis of reaction products and intermediates was performed, and the results were interpreted with a comprehensive kinetic model, developed through a first-principles approach, describing the oxidation of methane and ammonia, as well as both fuel interaction and NO<sub>x</sub> formation.

## 2. Experimental methodology

The co-oxidation of methane and ammonia was experimentally investigated using two different reactors (see additional details in Supplementary Material (SM1)) working close to atmospheric pressure, with helium as carrier gas. Mass flow controllers were used for reactor feeding (relative

uncertainty of  $\pm 0.5\%$  in flow). In a first set-up, experiments were performed in a fused silica JSR, a type of continuous stirred-tank reactor usually operated at steady state. JSRs were used for several gas-phase kinetic studies and the present JSR setup was already described in previous works [22-24]. It consisted of a spherical vessel with injection of the fresh mixture through four nozzles located at the center of the reactor, creating high turbulence resulting in homogeneity in composition and temperature. As a result, the JSR can be modeled as a perfectly stirred reactor. Its residence time was fixed at 1.5 s. The heating of the reactor was achieved through Inconel resistances, and the reaction temperature was measured with a K-type thermocouple located in a glass finger close to the center of the reactor (uncertainty of  $\pm 5$  K).

A second setup was used to investigate the co-oxidation of  $\text{CH}_4$  and  $\text{NH}_3$  at higher temperature (up to  $\sim 2000$  K) in a flow reactor (FR), consisting in an alumina tube (inner diameter of 4 mm and 100 cm in length) designed to approximate plug flow conditions with the Peclet numbers  $> 50$  (see SM1). The reactor was located horizontally in an electrically heated oven (Carbolite Gero). Temperature profiles were measured with a R-type thermocouple (profiles are provided in SM2). The isothermal reaction zone is located between 36 and 58 cm with a uniform temperature profile ( $\pm 30$  K). For each experiment, the residence time was fixed to about 25 ms in the central zone where the temperature can be considered constant. It must be noted that undesirable catalytic effects of the reactor wall were first observed in FR when using non recrystallized alumina.

The reactants and reaction products were analyzed using four diagnostics:

- Two gas chromatographs (GCs) were used for the quantification of carbon-containing species such as methane, carbon monoxide, carbon dioxide and the three  $\text{C}_2$  hydrocarbons (the carrier gas was helium). They were equipped with GSQ (JSR setup) and PlotQ (FR setup) capillary columns, respectively. Both included a Flame Ionization Detector (FID) preceded by a methanizer (for the reduction by  $\text{H}_2$  of oxygenated and nitrogenated functional groups over a heated nickel catalyst) allowing a better sensitivity for CO,  $\text{CO}_2$  and HCN detection than a thermal conductivity detector. Calibrations were performed using gaseous standards or using the “effective carbon number” method for carbon containing species [24].
- Nitric oxide (NO) and nitrogen dioxide ( $\text{NO}_2$ ) were detected in JSR and FR experiments using a dedicated NOx analyzer (Thermo Scientific Model 42i), based on chemiluminescence. This analyzer had two channels, one for the detection of nitric oxide in a direct and independent way, and a second one for the measure of the total NOx concentration. Calibrations were performed using gaseous standards.
- A continuous-wave Cavity Ring-Down Spectroscopy (cw-CRDS) cell coupled to the JSR by a sonic probe was used for ammonia quantification. This technique was previously successfully used for the detection of species, such as hydrogen peroxide during the oxidation of alkanes [25] and HONO during the oxidation of n-pentane doped with nitric oxide [26]. Ammonia has strong absorption lines in the wavelength range  $6637\text{--}6643\text{ cm}^{-1}$ , making the quantification accurate and providing a good sensibility. Cross sections were deduced from data recorded under non-reactive conditions.
- On-line mass-spectrometry was used to detect  $\text{NH}_3$ ,  $\text{N}_2$ ,  $\text{H}_2\text{O}$ ,  $\text{CH}_4$ ,  $\text{CO}_2$  and  $\text{O}_2$  during the co-oxidation of  $\text{CH}_4$  and  $\text{NH}_3$  in FR. Sampling was achieved through a capillary tube directly connecting the FR outlet and the analyzer. This technique requires the calibration of each species as there is no obvious relationship between their structures and their calibration factors. Gaseous

standards were used except for CO<sub>2</sub> and water, which were calibrated considering the reaction complete at the highest temperature.

- Fourier Transform InfraRed Spectroscopy was used to highlight the possible presence of N<sub>2</sub>O as this species has a strong absorption in the 400–4000 cm<sup>-1</sup> wavelength range. However, no N<sub>2</sub>O was observed during experiments, likely due to concentrations below the detection limit (estimated to 50 ppm at 2237.5 cm<sup>-1</sup>).

Relative uncertainties in mole fractions are ±5% for species detected by gas chromatography and NO. It is ±10% for ammonia quantified by CRDS, NO<sub>2</sub> and the species detected by online mass spectrometry.

### 3. Kinetic model

The kinetic model describing ammonia and methane oxidation and their mutual interaction was obtained by following a hierarchical methodology, i.e. the founding principle of the CRECK framework [27]. The mechanism relied on a core C<sub>0</sub>-C<sub>2</sub> module developed by Metcalfe et al. [28], on top of which the C<sub>3</sub> mechanism of Burke et al. [29] was added. Thermodynamic properties were taken from the database of Burcat and Ruscic [30].

NO<sub>x</sub> submechanism leveraged the recent work of Song et al. [22], where its capability to represent the sensitizing effects of both NO and NO<sub>2</sub> on CH<sub>4</sub> oxidation at lower temperatures had been demonstrated. This served as a basis for the development of this new ammonia oxidation mechanism, which was performed via an ab-initio evaluation of the ammonia decomposition and H-abstraction reactions. A full description of the mechanism construction and its wide-range validation can be found in the paper by Stagni et al. [7].

The complete mechanism is made up of 157 species and 2444 reactions, and is available under CHEMKIN format in SM3-5, along with thermodynamic and transport properties. For the sake of completeness, a wide-range validation in the conditions of interest is also reported in Figures S4–S12 in SM1.

### 4. Experimental results

In this work, the equivalence ratio ( $\Phi$ ) was defined considering CO<sub>2</sub>, water and NO as final combustion products from methane and ammonia oxidation. NO was considered rather than N<sub>2</sub>, since non-negligible amounts of NO were formed under the conditions of this study.

#### 4.1. Jet-stirred reactor

JSR experiments were performed over the temperature range 600–1200 K, at a residence time of 1.5 s, a pressure of 106.7 kPa, with inlet methane and ammonia mole fractions of 10,000 and 500 ppm, respectively, and at three equivalence ratios (0.5, 1 and 2). Two particular phenomena were observed during experiments, making the oxidation study of methane/ammonia mixtures tricky. The first was the occurrence of oscillation regimes under specific conditions (at the highest temperatures for the lean and stoichiometric mixtures). Mole fractions were not constant in time,

which was not compatible with the diagnostics used in this study. For this reason, the investigated temperature range is limited for some conditions in the results displayed hereafter. This phenomenon has been previously reported in literature for the oxidation of neat methane [31], and its kinetic foundations were explained in [32]. The second phenomenon was the occurrence of wall reactions strongly enhancing the ammonia consumption, although the reactor was made of fused silica. This problem was solved by treating the surface of the JSR before each experiment by flowing all gases but ammonia under reactive conditions.

Figure 1 displays the mole fractions of both reactants and main products. The temperature of the reactivity onset is very sensitive to the equivalence ratio: it is about 1000 K for the lean condition, 1075 K for the stoichiometric ones, and 1150 K in rich mixtures, according to the temperature dependence of the methane and ammonia mole fractions shown in Figure 1a–b. Figure 1a also displays  $\text{CH}_4$  mole fractions in the case of the oxidation of neat methane for comparison. Mole fractions are comparable to those of methane when doped with ammonia for the rich conditions, whereas the reactivity onset is anticipated ( $\sim 100$  K) by ammonia addition under lean conditions, and conversion is slightly enhanced in stoichiometric conditions.

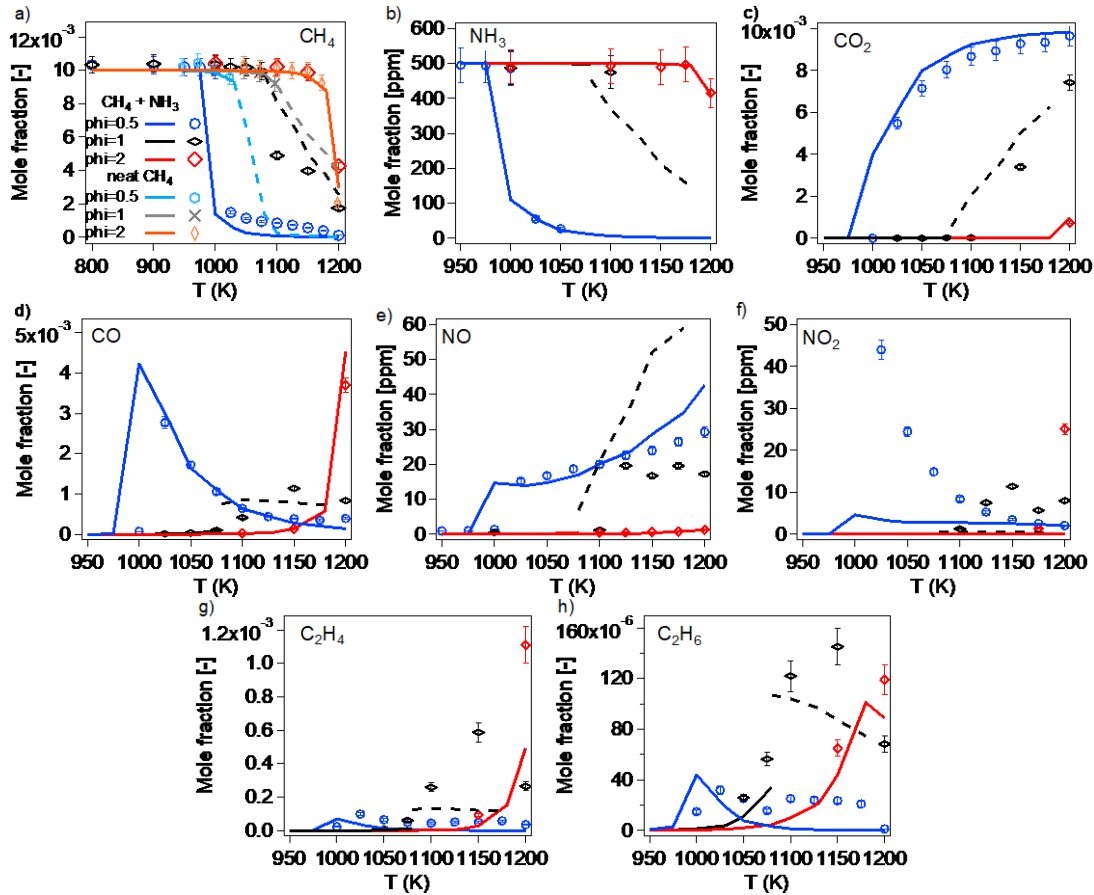


Figure 1. Mole fractions of reactants and main reaction products at a variable temperature and equivalence ratio in the JSR. Symbols: experiments. Lines: data computed with the model (dashed lines are averaged mole fractions due to oscillation regime).

The main carbon containing products are carbon monoxide, carbon dioxide, ethylene and ethane (Figure 1). Under lean conditions, carbon monoxide mole fractions peak at 1025 K. Above this

temperature, a decrease of the CO mole fraction is observed with a simultaneous increase of that of CO<sub>2</sub>. The mole fractions of ethylene and ethane remain low (less than 500 ppm). Larger equivalence ratios favor the formation of unburnt species.

Only two nitrogen-containing species were detected during this study: nitric oxide (NO) and nitrogen dioxide (NO<sub>2</sub>), but more N-containing species should be formed in significant amounts because the N-atom balance is not closed. This is likely due to the formation of N<sub>2</sub>, which was expected, but its detection was not possible because of interference in GC analyses. NO and NO<sub>2</sub> mole fractions are displayed in Figure 1e–f. Under lean conditions, the mole fractions of these last products increase simultaneously to ammonia depletion. NO<sub>2</sub> mole fraction already peaks at 1025 K and afterward decreases whereas that of NO continue to increase. Note that NO behaves closely to CO<sub>2</sub> whereas NO<sub>2</sub> behaves closely to CO.

Under stoichiometric conditions, oscillation behavior was detected above 1025 K. Beyond this temperature, data for ammonia are not accurate because oscillations are not compatible with the CRDS spectrum acquisition time of ammonia (about 30 min) and the in-situ sampling. Data recorded with the NO<sub>x</sub> analyzer and by GC, with a sampling strategy based on the injection of a defined volume accumulated on the larger time scale, can be considered as time averages. Oscillations seem to have a minor impact on species like methane, carbon monoxide and carbon dioxide. This is because the mole fractions of these species are larger compared to those of nitric oxide and nitrogen dioxide.

## 4.2. Flow reactor

FR experiments were performed over a temperature range significantly higher than in the JSR thanks to the use of a recrystallized alumina tube and an oven heating up to temperatures as high as ~2000 K. The two fuels, the oxidizer, and 11 reaction products were followed. Reaction products can be divided as follows:

- Species specific to methane oxidation: CO, CO<sub>2</sub>, C<sub>2</sub>H<sub>2</sub>, C<sub>2</sub>H<sub>4</sub>, C<sub>2</sub>H<sub>6</sub> and C<sub>3</sub>H<sub>6</sub>.
- Species specific to ammonia oxidation: N<sub>2</sub>, NO and NO<sub>2</sub>.
- Species common to both fuels: water and HCN.

Note that HCN is the only fuel cross-product whose formation was observed during these high temperature experiments. Mole fraction profiles are displayed in Figure 2. C-, N-, H- and O-atom balances were calculated for each temperature and are all in the range of 0.99±0.05 (see values in Table S4 in SM1).

The consumption of methane and ammonia becomes significant starting from ~1500 K and they are already totally consumed at ~1600 K. The two main products from the oxidation of methane are CO and CO<sub>2</sub>. CO peaks at 1573 K and is then progressively converted to CO<sub>2</sub> when the temperature increases. Ammonia is mainly converted to NO and N<sub>2</sub>, and NO/N<sub>2</sub> ratio slightly increases with temperature. Note that under these conditions, equilibrium calculations predict the formation of N<sub>2</sub> quasi exclusively. Small amounts of NO<sub>2</sub> were also observed on a very narrow range (between 1550 and 1600 K). A part of O<sub>2</sub> remains not consumed even at the highest

temperatures because of the formation of  $N_2$  from  $NH_3$  (the  $NH_3/O_2$  inlet ratio was calculated considering only NO as product to be sure to have enough oxygen for fully consuming methane). Other reaction products ( $C_2$  species,  $C_3H_6$  and HCN) are produced in small amounts and over a narrow temperature range as for  $NO_2$  (Figure 2e).

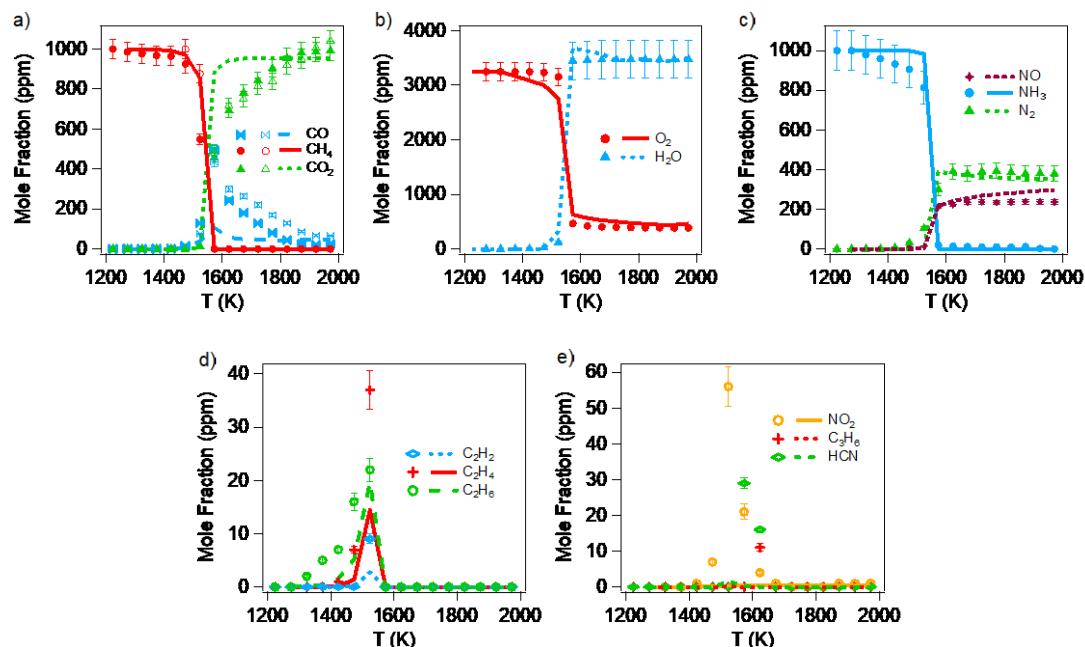


Figure 2. Mole fractions of the fuels and main reaction products recorded during the oxidation of methane and ammonia in the flow tube reactor ( $\Phi=1$ ). Symbols: experiments (close symbols in panel a) are for methane-ammonia co-oxidation, open symbols are for neat methane oxidation). Lines: data computed with the model.

## 5. Comparison between experimental and simulated results

Figures 1 and 2 compare the experimental data and model results. The kinetic model well predicts the temperature of the reactivity onset for both reactors as it can be seen for methane and ammonia in Figures 1 and 2. The temperature dependence of the conversion of both fuels is also well predicted, although the residual presence of methane after  $T = 1025$  K is underestimated. In the JSR, at  $\Phi=1$ , where oscillation behavior was detected above 1025 K, the mole fractions of methane (GC detection) reasonably agree with averaged computed mole fractions (dashed lines in Figure 1). The model predicts the anticipated reactivity of methane in presence of ammonia under lean conditions.

As far as JSR reaction products are concerned, mole fractions of carbon monoxide and of carbon dioxide are well predicted by the model at all equivalence ratios (even for the stoichiometric case for which oscillating computed mole fractions were averaged). Mole fractions of ethane and NO are also reproduced fairly well by the model. Discrepancies are observed for nitrogen dioxide for which the model under-estimates the formation, especially under lean conditions. This issue was also previously observed by Song et al. in the  $CH_4$  oxidation doped with NO [22]. For the rich case,



the signal detected for  $\text{NO}_2$  under these high temperature conditions is likely due to an interference with that of  $\text{HCN}$ , which is a typical high temperature product under rich conditions (whereas  $\text{NO}_2$  is usually produced at low-temperature oxidation), as already observed in [22].

In the FR, the agreement is also quite satisfactory for the main reaction products such as water,  $\text{NO}$  and  $\text{N}_2$ . Surprisingly, the model predicts a more abrupt increase of  $\text{CO}_2$  and decrease of  $\text{CO}$  mole fractions than in the experiments. This trend is also observed when studying the oxidation of neat methane (open symbols in Figure 2a), indicating that it is not due to the presence of ammonia in the feed of the reactor. According to a kinetic analysis performed at 1600 K, the second most sensitive reaction is  $\text{CO} + \text{OH} = \text{CO}_2 + \text{H}$  (after the branching reaction  $\text{H} + \text{O}_2 = \text{OH} + \text{O}$ ) the kinetic parameters of which are relatively well known. With the current mechanism there is no way to explain this deviation, as well as the pre-reaction of  $\text{NH}_3$  before ignition (which was also observed in [15] with different inlet mixtures). The model predicts negligible amounts of  $\text{NO}_2$ ,  $\text{C}_3\text{H}_6$  and  $\text{HCN}$  compared to the experiment.

## 6. Kinetic analysis

Rate-of-production and sensitivity analyses were performed to highlight the chemistry involved during the co-oxidation of methane and ammonia, and their mutual interactions. Figure 3 presents a rate analysis for fuel consumption (Figure 3a) and a sensitivity analysis for methane mole fraction (Figure 3b) performed under JSR conditions (944 K,  $\phi = 0.5$ , corresponding to conversions of 18% and 9% of methane and ammonia, respectively). Figure 4 displays a rate analysis for fuel consumption (Figure 4b) and a sensitivity analysis for methane mole fraction (Figure 4a) performed under FR conditions ( $\sim 1560$  K,  $\phi = 1$ , and an abscissa of 46 cm (length from the tube inlet) corresponding to methane and ammonia conversions of  $\sim 50\%$  and  $\sim 20\%$ , respectively).

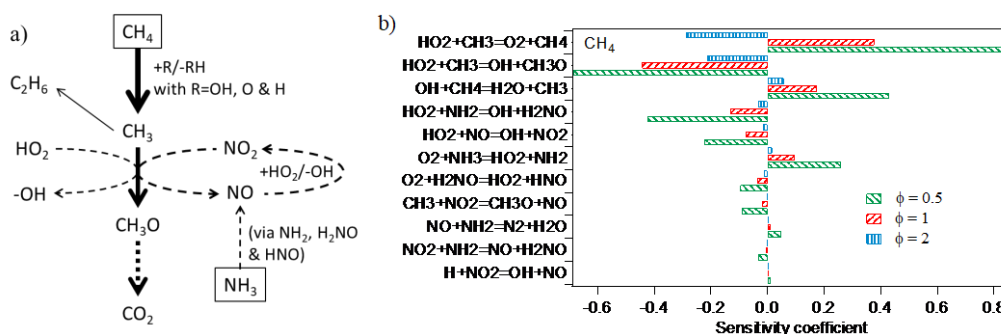


Figure 3. a) Consumption pathways of methane and ammonia, and b) sensitivity analysis for methane mole fraction at variable  $\Phi$  for  $\sim 1\%$   $\text{CH}_4$  conversion. Sensitivity coefficients are normalized with respect to the value of  $\text{H} + \text{O}_2 = \text{O} + \text{OH}$  (not included).

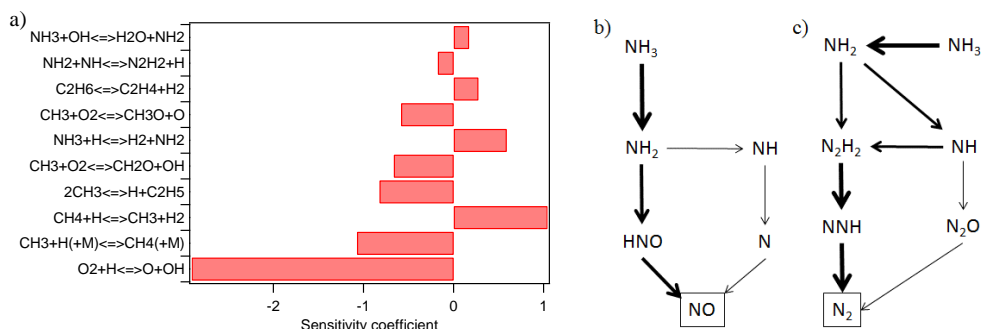


Figure 4. a) Sensitivity diagram for methane under the FR conditions. b) and c) Formation routes to NO and  $\text{N}_2$  ( $T = 1560 \text{ K}$ ,  $\Phi = 1$ ,  $x = 46 \text{ cm}$  (length from the tube inlet)). Arrow thickness is proportional to the reaction flux.

At low temperatures and under JSR conditions, the analysis shows that the consumption of methane starts with the classic H-atom abstraction reaction,  $\text{CH}_4 + \text{OH} = \text{CH}_3 + \text{H}_2\text{O}$ . The main consumption route of  $\text{CH}_3$  is  $\text{CH}_3 + \text{NO}_2 = \text{CH}_3\text{O} + \text{NO}$  (as in the case of the oxidation of methane doped with NO and  $\text{NO}_2$  [22]),  $\text{NO}_2$  coming from the reaction  $\text{NO} + \text{HO}_2 = \text{NO}_2 + \text{OH}$ . Minor channels are  $\text{CH}_3 + \text{HO}_2 = \text{CH}_3\text{O} + \text{OH}$  and the recombination reaction forming ethane. Afterwards, the reaction series leading to  $\text{CO}_2$ , via  $\text{CH}_3\text{O}$ ,  $\text{CH}_2\text{O}$ ,  $\text{CHO}$ ,  $\text{CO}$ , is not directly affected by the presence of ammonia. The central role of the  $\text{HO}_2$  radicals in converting  $\text{CH}_3$  to  $\text{CH}_3\text{O}$  is noteworthy, through both direct reaction with  $\text{CH}_3$  and indirectly by regenerating  $\text{NO}_2$  from NO. The main sources of  $\text{HO}_2$  radicals are the reactions  $\text{HCO} + \text{O}_2 = \text{CO} + \text{HO}_2$  and  $\text{H} + \text{O}_2(+M) = \text{HO}_2(+M)$ .

In these conditions, ammonia is mainly consumed by H-abstraction by  $\text{HO}_2$ , which is present in significant amounts at low temperatures. The high amounts of  $\text{HO}_2$  also cause the termination of  $\text{NH}_2$  radical, such as the reverse reaction prevails over the forward H-abstraction, and acts as a termination. This effect had already been noticed by Stagni et al. [7] in the oxidation of pure ammonia, although in this setup it does not affect reactivity to a significant extent (Figure 3b) because of the presence of methane in higher amounts.  $\text{NH}_2$  holds a key role in modifying the reactivity of pure methane: it reacts with NO and  $\text{NO}_2$ , and each of these two paths owns a branching and a terminating channel. The sensitivity analysis (Figure 3b), carried out at different  $\Phi$  for the same  $\text{CH}_4$  conversion (1%), highlights the importance of  $\text{H}_2\text{NO}$ , formed by both branching channels and by  $\text{NH}_2$  reaction with  $\text{HO}_2$ .  $\text{H}_2\text{NO}$  is then further oxidized to HNO and finally to NO (the chemistry of  $\text{H}_2\text{NO}$  is one of the biggest challenges in ammonia kinetics [21,32]). The interplay between  $\text{NO}_2$  and NO is also evident in the sensitivity analysis, since  $\text{NO}_2$  formation via  $\text{NO} + \text{HO}_2$  enhances reactivity, and vice versa for its disappearance via its reaction with H. Indeed,  $\text{NO}_2$  is the key molecule in sensitizing methane chemistry: the formation of the reactive methoxy radical ( $\text{CH}_3\text{O}$ ) triggers the oxidation process of methane, as already shown in [22]. Therefore, the two reactions  $\text{CH}_3 + \text{NO}_2 = \text{CH}_3\text{O} + \text{NO}$  and  $\text{NO} + \text{HO}_2 = \text{NO}_2 + \text{OH}$  act as a catalytic cycle enhancing the consumption of methane. Conversely, with a richer mixture, the importance of ammonia chemistry becomes less and less important, and the lower amount of  $\text{HO}_2$  stops the catalytic cycle. Thus, with increasing  $\Phi$ , the usual  $\text{CH}_4$  oxidation mechanism prevails, and sensitivity analysis shows that H-abstraction reactions and methyl conversion to methoxy govern the system reactivity.

Under FR conditions, there are fewer direct interactions between methane and nitrogenated species. Methane is still mainly consumed through H-abstractions by H, O and OH radicals.  $\text{CH}_3$  radicals mainly react with O-atoms to yield  $\text{CH}_2\text{O}+\text{H}$ , i.e. bypassing  $\text{CH}_3\text{O}$  chemistry, crucial at lower temperatures. The second most important  $\text{CH}_3$  reaction is the termination to ethane, and the third one is its interaction with NH forming  $\text{CH}_2\text{NH}+\text{H}$ . However, this does not have a significant impact on reactivity (Figure 4a). Formaldehyde reacts following the usual sequence to give  $\text{CO}_2$ .  $\text{CH}_2\text{NH}$  chemistry is not discussed here as it is not determining. The sensitivity diagram in Figure 4a shows that the reactivity is mainly governed by the chemistry of methane, whereas the impact of ammonia is minor, and limited to i) H-abstraction on ammonia itself, slowing down the reactivity since it subtracts active radicals for branching, and ii)  $\text{N}_2\text{H}_2$  formation from  $\text{NH}_2$  and NH, with consequent release of a H radical. Therefore, the oxidation paths of the two fuels is mostly governed by their independent interactions with the radical pool (H, O, OH).

As far as ammonia specific chemistry is concerned, the intermediate HNO plays a minor role under these high temperature conditions. The  $\text{NH}_2$  radical mainly gives NH. It also reacts back to ammonia and leads to  $\text{N}_2\text{H}_2$  by combination.  $\text{N}_2\text{H}_2$  is converted into  $\text{N}_2$ , one of the major reaction products, through NNH. The NH radical mainly reacts with  $\text{CH}_3$  yielding  $\text{CH}_2\text{NH}$ , while its second most important consumption route is to produce  $\text{N}_2\text{H}_2$ . It also yields  $\text{N}_2$  via  $\text{N}_2\text{O}$  and NO, another major reaction product, via N. Rate of production analysis shows that  $\text{N}_2\text{O}$  mostly acts as an intermediate species rather than as a final product, due to the high temperatures involved, causing its quick decomposition to  $\text{N}_2$  and O. Anyway, the main NO formation pathway is still through HNO, which is formed from  $\text{NH}_2$ , although it is a minor consumption pathway for this last species.

## Conclusions

In this work, the co-oxidation of methane and ammonia was experimentally and theoretically studied to investigate their mutual interactions in combustion processes. Experiments were performed in a jet-stirred reactor and in a newly developed flow tube reactor working up to  $\sim 2000$  K. Comparison of experimental data with simulations using a novel detailed kinetic model showed a satisfactory agreement for the reactivity and for the mole fractions of most reaction products. The kinetic analysis of the system shed light on the underlying causes of the  $\text{NH}_3$  promoting effect, and on the major role played by NO in anticipating methane reactivity at low temperature. Although the effect of NO as a reactivity enhancer had been already established in previous works [22], it was observed in the present work that even as an intermediate species in the ammonia oxidation path, it affects methane oxidation to a major extent, shifting the reactivity onset by up to  $\sim 100$  K, especially in the leanest conditions. This effect is not present at higher temperatures where the reactivity is mainly governed by fuel H-abstractions by OH, O and H. In this case, as soon as methane reacts, the radical pool necessary to trigger ammonia oxidation becomes available, such as the reactivity onset of the two fuels occurs at the same temperature, and is slightly anticipated with respect to pure  $\text{CH}_4$  mostly because of the higher amount of fuel.

## Acknowledgments

This work has received funding from the European Union H2020 (H2020-SPIRE-04-2016) under grant agreement n°723706.

## Supplementary material

- A word file named SM1 containing additional information about the experimental setups, atomic balance calculations, and additional model validations.
- A spreadsheet named SM2 with jet-stirred reactor and flow reactor experimental data.
- Three text files named SM3-5 containing thermodynamic properties, transport data and reactions under the Chemkin format.

## References

- [1] D.P.B.T.B. Strik, A.M. Domnanovich, P. Holubar, A pH-based control of ammonia in biogas during anaerobic digestion of artificial pig manure and maize silage, *Process Biochem.* 41 (2006) 1235–1238. <https://doi.org/10.1016/j.procbio.2005.12.008>.
- [2] R.O. Arazo, D.A.D. Genuino, M.D.G. de Luna, S.C. Capareda, Bio-oil production from dry sewage sludge by fast pyrolysis in an electrically-heated fluidized bed reactor, *Sustain. Environ. Res.* 27 (2017) 7–14. <https://doi.org/10.1016/j.serj.2016.11.010>.
- [3] H. Kobayashi, A. Hayakawa, K.D.K.A. Somarathne, E.C. Okafor, Science and technology of ammonia combustion, *Proc. Combust. Inst.* 37 (2019) 109–133. <https://doi.org/10.1016/j.proci.2018.09.029>.
- [4] J. Ikäheimo, J. Kiviluoma, R. Weiss, H. Holttinen, Power-to-ammonia in future North European 100 % renewable power and heat system, *Int. J. Hydrog. Energy.* 43 (2018) 17295–17308. <https://doi.org/10.1016/j.ijhydene.2018.06.121>.
- [5] H. Xiao, A. Valera-Medina, P.J. Bowen, Study on premixed combustion characteristics of co-firing ammonia/methane fuels, *Energy.* 140 (2017) 125–135. <https://doi.org/10.1016/j.energy.2017.08.077>.
- [6] A.J. Reiter, S.-C. Kong, Combustion and emissions characteristics of compression-ignition engine using dual ammonia-diesel fuel, *Fuel.* 90 (2011) 87–97. <https://doi.org/10.1016/j.fuel.2010.07.055>.
- [7] A. Stagni, C. Cavallotti, S. Arunthanayothin, Y. Song, O. Herbinet, F. Battin-Leclerc, T. Faravelli, An experimental, theoretical and kinetic-modeling study of the gas-phase oxidation of ammonia, *React. Chem. Eng.* 5 (2020) 696–711. <https://doi.org/10.1039/C9RE00429G>.
- [8] A.A. Konnov, I.V. Dyakov, J.D. Ruyck, Probe Sampling Measurements of NO in CH<sub>4</sub>+O<sub>2</sub>+N<sub>2</sub> Flames Doped with NH<sub>3</sub>, *Combust. Sci. Technol.* 178 (2006) 1143–1164. <https://doi.org/10.1080/00102200500296788>.
- [9] B. Li, Y. He, Z. Li, A.A. Konnov, Measurements of NO concentration in NH<sub>3</sub>-doped CH<sub>4</sub>+air flames using saturated laser-induced fluorescence and probe sampling, *Combust. Flame.* 160 (2013) 40–46. <https://doi.org/10.1016/j.combustflame.2012.10.003>.
- [10] B.A. Williams, J.W. Fleming, Radical species profiles in low-pressure methane flames containing fuel nitrogen compounds, *Combust. Flame.* 110 (1997) 1–13. [https://doi.org/10.1016/S0010-2180\(97\)00063-1](https://doi.org/10.1016/S0010-2180(97)00063-1).
- [11] I. Rahinov, A. Goldman, S. Cheskis, Absorption spectroscopy diagnostics of amidogen in ammonia-doped methane/air flames, *Combust. Flame.* 145 (2006) 105–116. <https://doi.org/10.1016/j.combustflame.2005.11.004>.
- [12] A. Garo, C. Hilaire, D. Puechberty, Experimental Study of Methane-Oxygen Flames Doped with Nitrogen Oxide or Ammonia. Comparison with Modeling, *Combust. Sci. Technol.* 86 (1992) 87–103. <https://doi.org/10.1080/00102209208947189>.

- [13] X. Han, Z. Wang, M. Costa, Z. Sun, Y. He, K. Cen, Experimental and kinetic modeling study of laminar burning velocities of NH<sub>3</sub>/air, NH<sub>3</sub>/H<sub>2</sub>/air, NH<sub>3</sub>/CO/air and NH<sub>3</sub>/CH<sub>4</sub>/air premixed flames, *Combust. Flame*. 206 (2019) 214–226. <https://doi.org/10.1016/j.combustflame.2019.05.003>.
- [14] E.C. Okafor, Y. Naito, S. Colson, A. Ichikawa, T. Kudo, A. Hayakawa, H. Kobayashi, Measurement and modelling of the laminar burning velocity of methane-ammonia-air flames at high pressures using a reduced reaction mechanism, *Combust. Flame*. 204 (2019) 162–175. <https://doi.org/10.1016/j.combustflame.2019.03.008>.
- [15] T. Mendiara, P. Glarborg, Ammonia chemistry in oxy-fuel combustion of methane, *Combust. Flame*. 156 (2009) 1937–1949. <https://doi.org/10.1016/j.combustflame.2009.07.006>.
- [16] V.J. Wargadalam, G. Löffler, F. Winter, H. Hofbauer, Homogeneous formation of NO and N<sub>2</sub>O from the oxidation of HCN and NH<sub>3</sub> at 600–1000°C, *Combust. Flame*. 120 (2000) 465–478. [https://doi.org/10.1016/S0010-2180\(99\)00107-8](https://doi.org/10.1016/S0010-2180(99)00107-8).
- [17] M. Barbas, M. Costa, S. Vranckx, R. Fernandes, Experimental and kinetic modeling study of CO and NO formation under oxy-fuel conditions, in: 2015: pp. 16–20.
- [18] O. Mathieu, M.M. Kopp, E.L. Petersen, Shock-tube study of the ignition of multi-component syngas mixtures with and without ammonia impurities, *Proc. Combust. Inst.* 34 (2013) 3211–3218. <https://doi.org/10.1016/j.proci.2012.05.008>.
- [19] S. Liu, C. Zou, Y. Song, S. Cheng, Q. Lin, Experimental and numerical study of laminar flame speeds of CH<sub>4</sub>/NH<sub>3</sub> mixtures under oxy-fuel combustion, *Energy*. 175 (2019) 250–258. <https://doi.org/10.1016/j.energy.2019.03.040>.
- [20] K.P. Shrestha, L. Seidel, T. Zeuch, F. Mauss, Detailed Kinetic Mechanism for the Oxidation of Ammonia Including the Formation and Reduction of Nitrogen Oxides, *Energy Fuels*. 32 (2018) 10202–10217. <https://doi.org/10.1021/acs.energyfuels.8b01056>.
- [21] P. Glarborg, J.A. Miller, B. Ruscic, S.J. Klippenstein, Modeling nitrogen chemistry in combustion, *Prog. Energy Combust. Sci.* 67 (2018) 31–68. <https://doi.org/10.1016/j.pecs.2018.01.002>.
- [22] Y. Song, L. Marrodán, N. Vin, O. Herbinet, E. Assaf, C. Fittschen, A. Stagni, T. Faravelli, M.U. Alzueta, F. Battin-Leclerc, The sensitizing effects of NO<sub>2</sub> and NO on methane low temperature oxidation in a jet stirred reactor, *Proc. Combust. Inst.* (2018). <https://doi.org/10.1016/j.proci.2018.06.115>.
- [23] L. Marrodán, Y. Song, M. Lubrano Lavadera, O. Herbinet, M. de Joannon, Y. Ju, M.U. Alzueta, F. Battin-Leclerc, Effects of Bath Gas and NO<sub>x</sub> Addition on n-Pentane Low-Temperature Oxidation in a Jet-Stirred Reactor, *Energy Fuels*. 33 (2019) 5655–5663. <https://doi.org/10.1021/acs.energyfuels.9b00536>.
- [24] M. Pelucchi, S. Namysl, E. Ranzi, A. Frassoldati, O. Herbinet, F. Battin-Leclerc, T. Faravelli, An experimental and kinetic modelling study of n-C<sub>4</sub>C<sub>6</sub> aldehydes oxidation in a jet-stirred reactor, *Proc. Combust. Inst.* 37 (2019) 389–397. <https://doi.org/10.1016/j.proci.2018.07.087>.
- [25] C. Bahrini, O. Herbinet, P.-A. Glaude, C. Schoemaecker, C. Fittschen, F. Battin-Leclerc, Quantification of Hydrogen Peroxide during the Low-Temperature Oxidation of Alkanes, *J. Am. Chem. Soc.* 134 (2012) 11944–11947. <https://doi.org/10.1021/ja305200h>.
- [26] L. Marrodán, Y. Song, O. Herbinet, M.U. Alzueta, C. Fittschen, Y. Ju, F. Battin-Leclerc, First detection of a key intermediate in the oxidation of fuel + NO systems: HONO, *Chem. Phys. Lett.* 719 (2019) 22–26. <https://doi.org/10.1016/j.cplett.2019.01.038>.
- [27] E. Ranzi, A. Frassoldati, R. Grana, A. Cuoci, T. Faravelli, A.P. Kelley, C.K. Law, Hierarchical and comparative kinetic modeling of laminar flame speeds of hydrocarbon and oxygenated fuels, *Prog. Energy Combust. Sci.* 38 (2012) 468–501. <https://doi.org/10.1016/j.pecs.2012.03.004>.
- [28] W.K. Metcalfe, S.M. Burke, S.S. Ahmed, H.J. Curran, A Hierarchical and Comparative Kinetic Modeling Study of C<sub>1</sub> – C<sub>2</sub> Hydrocarbon and Oxygenated Fuels, *Int. J. Chem. Kinet.* 45 (2013) 638–675. <https://doi.org/10.1002/kin.20802>.
- [29] S.M. Burke, U. Burke, R. Mc Donagh, O. Mathieu, I. Osorio, C. Keese, A. Morones, E.L. Petersen, W. Wang, T.A. DeVerter, M.A. Oehlschlaeger, B. Rhodes, R.K. Hanson, D.F. Davidson, B.W. Weber, C.-J. Sung, J. Santner, Y. Ju, F.M. Haas, F.L. Dryer, E.N. Volkov, E.J.K. Nilsson, A.A. Konnov, M. Alrefae, F. Khaled, A. Farooq,

- P. Dirrenberger, P.-A. Glaude, F. Battin-Leclerc, H.J. Curran, An experimental and modeling study of propene oxidation. Part 2: Ignition delay time and flame speed measurements, *Combust. Flame*. 162 (2015) 296–314. <https://doi.org/10.1016/j.combustflame.2014.07.032>.
- [30] A. Burcat, B. Ruscic, Chemistry, T.-I.I. of Tech, Third millenium ideal gas and condensed phase thermochemical database for combustion (with update from active thermochemical tables), Argonne National Lab. (ANL), Argonne, IL (United States), 2005. <https://doi.org/10.2172/925269>.
- [31] M. Lubrano Lavadera, Y. Song, P. Sabia, O. Herbinet, M. Pelucchi, A. Stagni, T. Faravelli, F. Battin-Leclerc, M. de Joannon, Oscillatory Behavior in Methane Combustion: Influence of the Operating Parameters, *Energy Fuels*. 32 (2018) 10088–10099. <https://doi.org/10.1021/acs.energyfuels.8b00967>.
- [32] A. Stagni, Y. Song, L.A. Vandewalle, K.M. Van Geem, G.B. Marin, O. Herbinet, F. Battin-Leclerc, T. Faravelli, The role of chemistry in the oscillating combustion of hydrocarbons: An experimental and theoretical study, *Chem. Eng. J.* 385 (2020) 123401. <https://doi.org/10.1016/j.cej.2019.123401>.